New Pyridine Dicarbene Ligands with Ring Expanded NHCs and their Nickel and Chromium Complexes

Evangelos Papangelis, Katrin Pelzer, Christophe Gourlaouen, Dominique Armspach, Pierre Braunstein, Andreas A. Danopoulos, Corinne Bailly, Nikolaos Tsoureas, Dimitrios Triantafyllos Gerokonstantis

CHEMISTRY
AN ASIAN JOURNAL
www.chemasianj.org

Accepted Article

Title: New Pyridine Dicarbene Ligands with Ring Expanded NHCs and their Nickel and Chromium Complexes

Authors: Evangelos Papangelis, Katrin Pelzer, Christophe Gourlaouen, Dominique Armspach, Pierre Braunstein, Andreas A. Danopoulos, Corinne Bailly, Nikolaos Tsoureas, and Dimitrios Triantafyllos Gerokonstantis

To be cited as: *Chem. Asian J.* **2024**, e202400169

Link to VoR: https://doi.org/10.1002/asia.202400169

A Journal of

ACES Asian Chemical Editorial Society

WILEY VCH

10.1002/asia.202400169

WILEY VCH

RESEARCH ARTICLE

New Pyridine Dicarbene Pincer Ligands with Ring Expanded NHCs and their Nickel and Chromium Complexes

Evangelos Papangelis,[a] Katrin Pelzer,[b] Christophe Gourlaouen,[c] * Dominique Armspach,[b] Pierre Braunstein,[b] * Andreas A. Danopoulos,[a] * Corinne Bailly,[d] Nikolaos Tsoureas[a] and Dimitrios Triantafyllos Gerokonstantis[e]

This paper is dedicated to Prof. Andy Hor, Prof. Xianjun Loh and Dr. Yun Zong from Agency for Science, Technology and Research (A*STAR), Singapore, Prof. Fuwei Li from University of Chinese Academy of Sciences, China, Prof. Guoqin Xu from National University of Singapore, Singapore and Prof. Jian-Ping Lang from Soochow University, Suzhou, China, for their outstanding contributions to chemistry and long-lasting friendship.

[a] E. Papangelis, Prof. A. A. Danopoulos, Prof. N. Tsoureas
Inorganic Chemistry Laboratory, Department of Chemistry
National and Kapodistrian University of Athens
Panepistimiopolis Zografou, 15771 Athens, Greece
E-mail: adanop@chem.uoa.gr

[b] Dr. K. Pelzer, Prof. D. Armspach, Prof. P. Braunstein,
Equipe Confinement Moléculaire et Catalyse, Institut de Chimie de Strasbourg, UMR 7177 CNRS,
Université de Strasbourg,
4, rue Blaise Pascal, CS 90032, 67081 Strasbourg Cedex, France
E-mail: d.armspach@unistra.fr; braunstein@unistra.fr

[c] Dr. C. Gourlaouen
Laboratoire de Chimie Quantique, Institut de Chimie de Strasbourg, UMR 7177 CNRS,
Université de Strasbourg,
4, rue Blaise Pascal, CS 90032, 67081 Strasbourg Cedex, France
E-mail: gourlaouen@unistra.fr

[d] Dr. C. Bailly
Fédération de Chimie "Le Bel" - UAR2042
BP 296R8
1, rue Blaise Pascal, 67008 Strasbourg Cedex, France
E-mail: c.bailly@unistra.fr

[e] Dimitrios Triantafyllos Gerokonstantis
Laboratory of Analytical Chemistry, Department of Chemistry,
National and Kapodistrian University of Athens,
Panepistimiopolis Zografou, 15771 Athens, Greece
E-mail: akisgerok@chem.uoa.gr

Supporting information for this article is given via a link at the end of the document.

Abstract: The pincer complexes [Ni^{II}Br(**CNC**)]Br (**4**), [Cr^{III}Br$_3$(**CNC**)] (**5a**) and [Cr^{III}Br$_{2.3}$Cl$_{0.7}$(**CNC**)] (**5b**), where **CNC** = 3,3'-(pyridine-2,6-diyl)bis(1-mesityl-3,4,5,6-tetrahydropyrimidin-2-ylidene), were obtained from the novel ligand **CNC**, generated *in situ* from the precursor **(CHNCH)Br$_2$** and [Ni^{II}Br$_2$(PPh$_3$)$_2$] or from [Cr^{II}{N(SiMe$_3$)$_2$}$_2$(THF)$_2$] and **(CHNCH)Br$_2$** by aminolysis, respectively. The tetrahedrally distorted square planar ($\tau_4 \cong 0.30$) geometry and the singlet ground state of Ni in **4** were attributed to steric constraints of the **CNC** backbone. Computational methods highlighted the dependence of the coordination geometry and the singlet-triplet energy difference on the size of the N-substituent of the tetrahydropyrimidine wingtips and contrasted it to the situation in 5-membered imidazolin-2-ylidene pincer analogues. The octahedral Cr^{III} metal center in **5a** and **5b** is presumably formed after one electron oxidation from CH_2Cl_2. **4**/MAO and **5a**/MAO were catalysts of moderate activity for the oligomerization and polymerization of ethylene, respectively. The analogous **(CH^N^CH)Br$_2$** precursor, where **(CH^N^CH)** = 3,3'-(pyridine-2,6-diylbis(methylene))bis(1-mesityl-3,4,5,6-tetrahydropyrimidin-1-ium), was also prepared, however its coordination chemistry was not studied due to the inherent instability of the resulting free **C^N^C** ligand.

Introduction

The study of chemical (structure, stoichiometric and catalytic reactivity), physical (photophysical, magnetic), biological and medicinal properties of metal complexes comprising one or more N-heterocyclic carbene (NHC) donors is a topical area of research, in particular with pincer-type ligand designs.[1],[2] In addition to the precise spatial tuning of the pincer architecture, the electronic and steric modulation of the NHC group(s) constitute attractive

10.1002/asia.202400169

RESEARCH ARTICLE

features to design, develop and tune functional complexes.[1j, 3] Accumulating evidence, also originating from diverse computational methodologies, points to the versatility of the NHC functionality in modulating the σ-donor and π-donor/acceptor interactions with the metal center. Towards this end, manipulation of the energies of the NHC HOMO and LUMO (and the respective energy difference between them) are instrumental. [1j, 3a, 3b, 4] The nature of the heterocycle, where the C^{NHC} is integrated in, is crucial for this purpose; thus, the σ-donation combined with the minimal π-acceptance of the imidazol- and imidazolin-based NHC functionalities are compared and contrasted to the pronounced σ-donation of the mesoionic NHCs and the σ-donation and π-acceptance of the Ring Expanded (RE) and cyclic Alkyl Amino Carbene (cAAC) NHCs.[5] Therefore, a good scope for the NHC selection could be in place to differentially (de)stabilize metal oxidation states, M–C^{NHC} and M–coligand interactions, metal nucleophilicity, promote/suppress lability *etc*. As part of a pincer ligand design, NHC functionalities can be installed at the wingtip(s) or bridgehead and subjected to the constraints of the rigid ligand structure, further modulating π-interactions *via* variation of torsion angles and steric interactions of the constituent functionalities.[6] In this respect, the magnitude of the N–C^{NHC}–E (E = heteroatom, usually N or C) angle can covertly accentuate the steric demands of the NHC functionality(ies) through enforcing distal bulky substituents to proximal positions. Despite the above mentioned options offered by the NHC functionality as a ligand building block, the majority of the studies with pincer ligand systems are based on the usage of 5-membered imidazol- and, to a lesser extent, imidazolin-based NHCs as side arms (type **I** in Fig. 1).[1a, 1c, 1i, 1j] In a limited number of studies mesoionic triazol-based wingtips (type **II** in Fig. 1) have been employed;[7] in contrast, wingtips based on the RE-NHCs (type **III** in Fig. 1) are unknown.[8] Interestingly, the picture regarding the nature of the NHC as bridgehead functionality shows more abundant usage of RE-6 NHCs, that have led to remarkable structural and reactivity differences compared to analogous 5-membered moieties (in particular, with donor atoms $OC^{NHC}O$ of aryloxide,[9] $NC^{NHC}N$ of pyridine or imine,[10] $PC^{NHC}P$[11] of dialkyl- or diaryl-phosphane). Herein, we report the synthesis of pyridine dicarbene pincer (pro)-ligands featuring RE-6 NHC wingtips (type **III**, E = N) and their usage in accessing Ni and Cr complexes of catalytic relevance. In the present study, the distinctive steric profile of the RE-6 NHC wingtip was manifested as (tunable) geometrical distortion at the metal with ground state electronic structure implications.

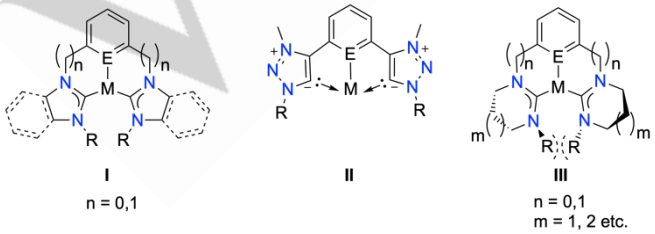

Figure 1. Common (type **I**, E = N, C *etc*.) and known (type **II**, E = N) symmetrical pincer ligand designs with NHC wingtips; type **III**, (E = N, n = 0, 1, m = 1) is the subject of this paper.

Results and Discussion

Proligand and Ligand Synthesis

The synthetic strategy to access the precursors **(CHNCH)Br₂** and **(CH^N^CH)Br₂** is depicted in Scheme 1. Although it should be general enough to accommodate any aromatic substituent at the six membered tetrahydropyrimidine, the choice of the mesityl group was dictated by the increased sterics anticipated in the resultant **CNC** complexes due to the obtuse N–C^{NHC}–N angle.

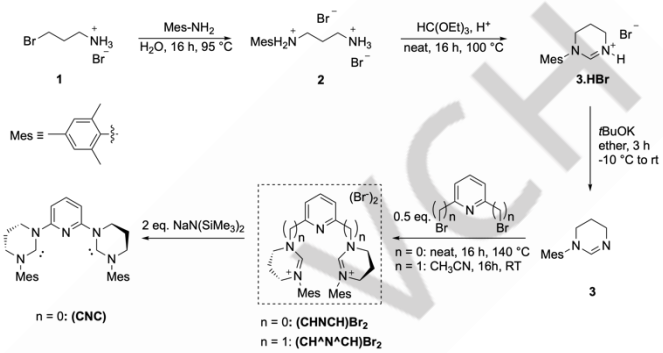

Scheme 1. The synthetic sequence leading to the pro-ligands **(CHNCH)Br₂** and **(CH^N^CH)Br₂** and the ligand **CNC**.

All steps in Scheme 1 proceed with good to excellent isolated yields at multigram scale. The proligands were isolated as colourless powders and characterized spectroscopically (see Experimental). Deprotonation of **(CHNCH)Br₂** with two equivalents of $NaN(SiMe_3)_2$ led to the pincer ligand **CNC** which could be isolated as an oily substance; it was stable at room temperature in C_6D_6 for at least 24 h, and was characterized by ^1H and $^{13}C\{^1H\}$ NMR spectroscopies. Although the NMR spectra were in agreement with the symmetric structure proposed for **CNC**, it was impossible to observe in the $^{13}C\{^1H\}$-NMR spectrum a signal assignable to the carbene carbon C^{NHC}, despite longer acquisition times and pulse delays to complete relaxation. In contrast, attempts to isolate at room temperature and characterize **C^N^C** were not successful and its future use for complexation reactions presumably should not be based on its *in situ* generation and trapping with metal precursors, but on 'coordinated base' methodologies or other C–H metalation protocols. Lastly, despite **CNC** being stable (*vide supra*), its long-term storage was avoided and for using it in metal complex syntheses, *in situ* generation in the presence of metal precursors was favored.

Computational Studies on the CNC Ligand

Since the molecular structure determination of **CNC** by X-ray diffraction methods was impossible due to the lack of crystallinity (*vide supra*), gaining insight into its metrical data, preferred conformation(s), stability and electronic structure were attempted by computational methods. According to DFT calculations, the computed **CNC(DFT)** in the gas phase can adopt three energetically unequal conformations (**A**, **B**, **C**), that differ in the relative orientation of the heterocyclic rings, where the two C^{NHC}

10.1002/asia.202400169

and the one N^{pyr} lone pair bearing atoms are located (Scheme 2). In the most stable conformer **C** repulsions between neighbouring lone pairs are minimized. Cartesian coordinates and selected metrical data of the three optimized structures are given in the Supporting Information (Tables S3, S5 and S6).

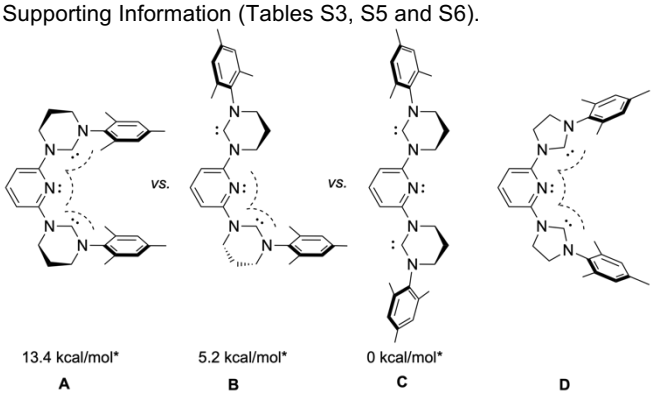

Scheme 2. The three conformers of **CNC(DFT)**: **A**: all *syn* lone pairs; **B**: *syn*, *anti* lone pairs; **C**: all *anti* lone pairs. The all *syn* conformer **D** was employed in computations for comparison purposes (see text for details). * The numbers denote the Gibbs free energies; the energy of conformer **C** was set to 0.0.

The singlet-triplet energy difference $\Delta E_{S\text{-}T}$ and the energy of the HOMO of the conformer **A** (resembling best the metal-bound conformation of the ligand) was computed at *ca.* -2.11 eV and -6.91 eV, respectively. In comparison, the $\Delta E_{S\text{-}T}$ and the energy of the HOMO of the relevant pincer ligand **D** with 5-membered NHCs were calculated at *ca.* -3.55 eV and -7.48 eV respectively, confirming the superior σ-donor characteristics of **A** when bound to a metal center; the energies of the LUMO in **A** and **D** are comparable (see Supporting Information, Table S9).

Interestingly, in addition to the difference of the magnitude of the $\Delta E_{S\text{-}T}$ there are disparities in the *nature* of the computed HOMOs, LUMOs and SOMOs of **A** and **D** in their singlet and triplet states: (i) in the singlet states, although in both **A** and **D** the nature of the HOMOs has clearly C^{NHC} and N^{pyr} lone pair character, in the HOMO of **D** there is significant contribution of the *π* system of the pyridine, which is almost absent in **A**; conversely, the LUMOs of both **A** and **D** have C^{NHC} and pyridine π character; (ii) moreover, in the triplet state in **A,** the energetically highest SOMO that displays C^{NHC} character, featuring two degenerate minima, each being localized on one of the RE-NHCs, results in the pyramidalization of one of the corresponding RE-NHC group (Figure 2). Conversely, π pyridine character, and 'dearomatization' of the pyridine are two features found in the triplet state in **D** (see also Supporting Information, Table S10). Recently, substantial localization of spin density in the π system of the pyridine bridgehead in radical anions of imidazol-2-ylidene analogues of **D** was experimentally observed and computationally demonstrated.[12]

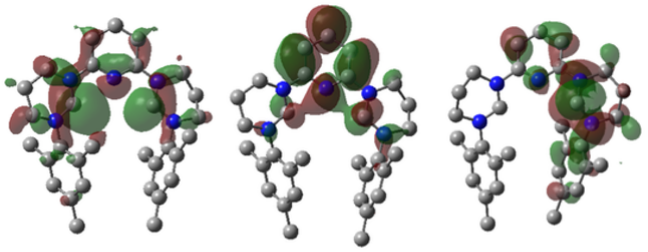

Figure 2 MOs of **A** (from left to right): HOMO, LUMO of the singlet state and SOMO of the triplet state.

Ni and Cr Complexes with the CNC Ligand

In view of our interest in the catalytic oligomerization of ethylene,[13] we employed the ligand **CNC** to access Cr and Ni complexes that are of relevance to this reaction (*vide infra*). The synthetic methods employed to access the well-defined complexes **4**, **5a** and **5b** are given in Scheme 3.

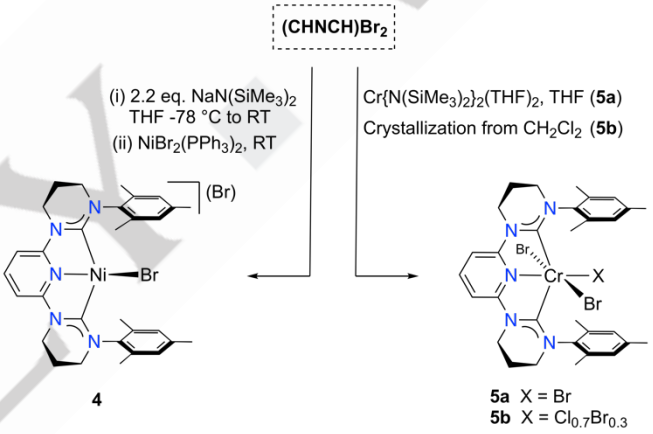

Scheme 3. Synthesis of Ni^{II} and Cr^{III} complexes with the **CNC** ligand.

The orange, diamagnetic Ni complex **4** was obtained in good yields (*ca.* 60%) by the reaction of the *in situ* generated **CNC** with $[NiBr_2(PPh_3)_2]$. In contrast, the pink-purple, paramagnetic complex **5a** was obtained in moderate yields (*ca.* 57%) after metalation of the **CNC** by aminolysis of $[Cr^{II}\{N(SiMe_3)_2\}_2(THF)_2]$ with the precursor **(CHNCH)Br$_2$** in THF, extraction into CH_2Cl_2 and isolation by solvent evaporation; the mechanism of the one electron oxidation of the metal and the origin of the third bromide co-ligand in **5a** is vague. Attempts to crystallize **5a** by pentane diffusion into a CH_2Cl_2 solution over one week led to the isolation of **5b** in the form of pink-purple crystals. The molecular structures of complexes **4** and **5b** determined crystallographically are shown in Figures 3 and 4 with important metrical data given in the caption of the Figures.[14] Noticeably, diamagnetic **4** was amenable to study by ^{1}H-NMR spectroscopy, while **5a** was silent in both ^{1}H-NMR and X-band EPR spectroscopy, in agreement with the presence of a high spin Cr^{III} center.[15]

10.1002/asia.202400169

RESEARCH ARTICLE

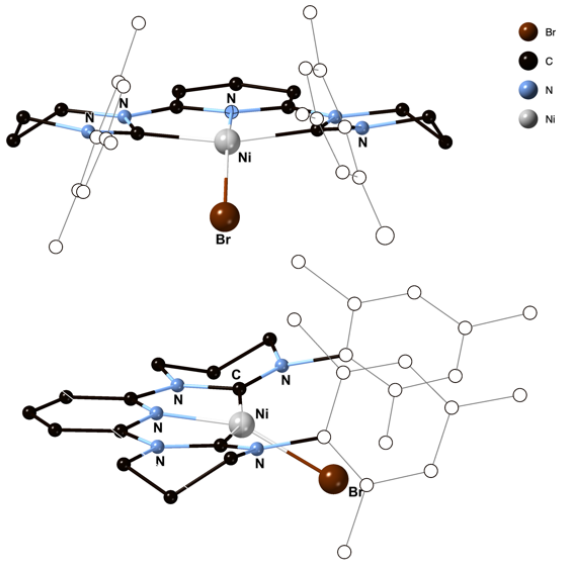

Figure 3. Two views of one of the two cations in the asymmetric unit of **4**; the second cation, two bromide anions, one toluene molecule and hydrogen atoms are omitted for clarity. Important metrical data (Å and °) are: Ni–N^{pyr} = 1.810(8). Ni–C^{NHC} = 1.942(10) and 1.958(10), Ni–Br = 2.2816(15), Br–Ni–N^{pyr} = 155.5(3), C^{NHC}–Ni–C^{NHC} = 162.0(4), C^{NHC}–Ni–N^{pyr} = 81.7(4) and 82.2(4), C^{NHC}–Ni–Br = 98.6(3) and 99.4(3), N–C^{NHC}–N = 119.4(9); the second cation in the asymmetric unit shows very similar metrical data (see also Supporting Information, Table S1).

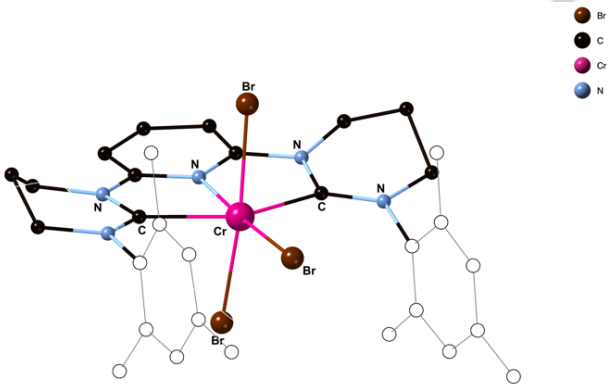

Figure 4. View of the molecular structure of **5b**; one CH_2Cl_2 molecule and hydrogen atoms are omitted for clarity. Important metrical data (Å and °) are: Cr–N^{pyr} = 1.998(2), Cr–C^{NHC} = 2.172(2) and 2.170(2), Cr–Br = 2.413(8), 2.4818(5) and 2.5016(5), Br–Cr–N^{pyr} = 177.4(2), C^{NHC}–Cr–C^{NHC} = 153.81(7), N–C^{NHC}–N = 116.66(19) (See also supporting information). The halogen atom site *trans* to the N^{pyr} is partially occupied by Br (30%) and Cl (70%); only the former is depicted for clarity (see also Supporting Information, Table S1).

The coordination geometry at Ni in **4** deviates substantially from the expected square planar ($\tau_4 \cong 0.30$),[16] whereas the bromide co-ligand is situated *ca.* 1.30 Å above the plane defined by the three other donors (C^{NHC} and N^{pyr}); the Ni center is only 0.16 Å above this plane. Both tetrahydropyrimidine six-membered rings adopt a half-chair conformation, thus maintaining the approximate C_s symmetry of the complex (relative to the plane defined by the N^{pyr}–Ni–Br), also in order to alleviate requirements arising from the planarity of the N–C^{NHC}–N substructure. The structural features of **4** are to be contrasted with those of the analogous complex with the five-membered (benz)imidazol-2-ylidene pincer already reported (imidazol, wingtip substituents: Me,[17] DiPP,[18] Mes,[19] benzimidazol: ^{n}Bu[20]) where virtually planar environments around the Ni^{II} centers are observed. The Ni–C^{NHC} bond distances in **4** are marginally longer than those reported for Ni^{II}-imidazol-2-ylidene complexes, possibly due to steric reasons (see Supporting Information, Table S2). In complex **5b** the metal adopts an octahedral coordination geometry. Here too, the two tetrahydropyrimidine six-membered rings of the pincer adopt half-chair conformation and an approximate C_s symmetry of the complex (relative to the plane defined by the N^{pyr}–Cr–Br_2) is obtained. The Cr–C^{NHC} bond distances in **5b** are in the range reported for the other pyridine dicarbene Cr complexes, *i.e.* (2.087(6), and 2.120(6) for Cr^{III} [21]), (2.125(12) and 2.122(10) for Cr^{II} [22]).

Computational Studies on the Geometric and Electronic Structure of the [Ni(CNC)X]$^+$ Analogues

In order to get insight into the factors that may be responsible for the unusual geometry around the Ni center in **4**, DFT calculations were undertaken. Thus, the computed structure of the cation in the singlet state **4BrMes^S** is in good agreement with the experimental and replicates the unusual features observed. In order to probe whether steric interactions could be held responsible for the structure of **4BrMes^S**, the structures of additional cations were computed: (i) with different NHC substituents (*i.e.* H, Me, adamantyl (Ad)), and (ii) with X coligands differing in size (Cl, Br, I). From the optimized structures were extracted: (i) the geometric parameter τ_4 and (ii) the concomitant energy difference E_T-E_S = ΔE_{TS} and used to quantify the departure from the square planar coordination geometry and the nature of the ground state electronic structure, respectively; the results are combined in Table 1.

Table 1. Computed structural and electronic parameters of the cation in **4** as a function of the wingtip substituent R and the halide coligand.[a]

Complex[b]	Spin Multiplicity	τ_4[16]	ΔE_{TS}[c]
4ClMes^S	Singlet	0.30	7.7
4ClMes^T	Triplet	0.71	
4BrMes^S	Singlet	0.33	7.0
4BrMes^T	Triplet	0.70	
4IMes^S	Singlet	0.40	4.6
4IMes^T	Triplet	0.72	
4BrH^S	Singlet	0.12	27.9

10.1002/asia.202400169

4BrH^{T}	Triplet	0.35	
4BrMe^{S}	Singlet	0.32	11.6
4BrMe^{T}	Triplet	0.56	
4BrAd^{S}	Singlet	0.45	-6.7
4BrAd^{T}	Triplet	0.68	
ImidClMes^{S}[d]	Singlet	0.12	14.5
ImidClMes^{T}[d]	Triplet	0.70	

[a] For the computation methodology see the Supporting Information; [b] The notations **4XR^{S}** and **4XR^{T}** refer to computed structures with R wingtip substituent, X coligand in the singlet or triplet states, respectively; [c] in kcal/mol; [d] **ImidClMes^{S}** and **ImidClMes^{T}** refer to computed structures of pyridine bis(imidazolin-2-ylidenes) with Mes wingtip substituent, Cl coligand in the singlet or triplet state, respectively.

Thus, when the substituents R at the wingtips are either Me, Mes or Ad, the Ni in the corresponding complex cations is in a distorted square planar environment with increasing τ_4 values as the steric bulk of the R group becomes larger. Conversely, when R = H, (**4BrH^{S}**), minimal distortion is observed ($\tau_4 \cong 0.12$). Moreover, increasing the size of the halide co-ligand also results in increased distortion away from the square planar.

This picture is further clarified by perusal of the steric maps derived after calculations of the % buried volume and its spatial distribution by employing the *SambVca* web toolkit[3c] and cartesian coordinates obtained experimentally (**4**) or by DFT methodology (as in Table 1); full details and representative results are found in the Supporting Information (Figure S18) and Figure 5, respectively.

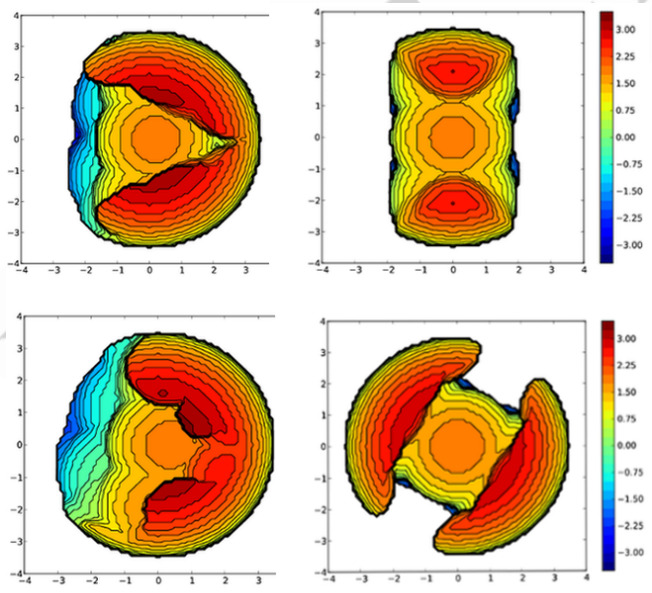

Figure 5 Steric maps of computed structures of the cations (from top left clockwise): **4BrMes^{S}**, **4BrH^{S}**, **ImidClMes^{S}** and **4BrAd^{S}**; the origin of the cartesian coordinates is at the Ni, the *z*-axis and the *xz*-plane coincide with the Ni–N^{pyr} vector and the C^{NHC}–N^{pyr}–C^{NHC} plane, respectively.

Finally, the calculations indicated that increased distortion from the square planar geometry results in smaller triplet-singlet energy difference ΔE_{TS}; in the calculated complexes with the bulkiest R (*i.e.* in **4BrAd**), the triplet is stabilized *vs.* the singlet state (by -6.7 kcal/mol). For the sake of comparison, DFT calculations were implemented on the analogous imidazolin-2-ylidene pincer complex (R = Mes), showcasing that it neither exhibits the aforementioned distortion ($\tau_4 \cong 0.12$) nor a narrow triplet-singlet energy difference ($\Delta E_{TS} \cong 14.5$ kcal/mol). The disparate features were attributed to the wider N–C^{NHC}–N angles of the RE-NHCs that force the NHC substituents (R) to close proximity with each other and the metal center (the calculated average ∢N–C^{NHC}–N in cations with RE-6 and the corresponding imidazol-2-ylidenes were *ca*. 117° and 104° respectively).

Catalytic Studies

Ligand design is paramount for tuning the activity and selectivity of Ni- and Cr-based ethylene oligomerization/polymerization catalysts. In particular, selectivities such as formation of oligomers *vs.* polymers, α-olefins *vs.* internal and branched alkenes are of high industrial interest and as a result many studies have been dedicated to the understanding of the reaction mechanisms at work.[23] So far, pyridine bis(imidazol-2-ylidene) Ni complexes activated with organoaluminium compounds have not been studied for their ability to catalyze alkene oligomerization/polymerization reactions; moreover, pyridine bis-imidazol-2-ylidene chromium complexes have been claimed to behave as efficient catalysts for ethylene oligomerization.[21, 24] To extend the scope of CNC-type pincer ligands, the complexes **4** and **5a** were tested for these reactions. A summary of the results obtained is given in Table 2.

Table 2. Summary of the catalytic oligo-(poly)-merization studies using **4** and **5a**.

Entry	Cat	TOF[a]	%C$_4$[b]	%C$_6$[b]	%C$_8$[b]	%C$_{10}$[b]	%PE
I	**4**	20504	70(48)	21(20)	6(21)	2(0)	-
II[c]	**4**	-	73(5)	24(2)	3(22)	-	-
III[d]	**4**	7022	60(45)	29(11)	9(3)	2(0)	-
IV	**5a**	8744[e]	3(100)	5(100)	2(100)	-	90
V	**5a**	728[e]	1(100)	-	-	-	100
VI[f]	**5a**	18206[e]	2(100)	1.5(100)	1(100)	0.5(95)	95

[a] Turnover frequency in: (mol C_2H_4)·(mol complex·h)$^{-1}$. [b] Percentage of olefin-product fractions with chain number of C atoms as indicated by the index (numbers in parentheses indicate the percentage of linear α-olefins); [c] 1 bar of C_2H_4 and 30 min run; [d] Initial temperature = 60 °C; [e] Turnover frequency was calculated only for the polymerization; [f] 20 bar C_2H_4.

All catalytic tests were conducted in chlorobenzene because the complexes are poorly soluble in toluene. It is evident that both **4**

10.1002/asia.202400169

and **5a** exhibit moderate activity[25] in terms of ethylene conversion, leading respectively to a mixture of oligomers and polymers with traces of oligomers, respectively. Although **5a** is predominantly a polymerization catalyst, the small amounts of oligomers detected turned out to be exclusively α-olefins. The polyethylene obtained was insoluble at room temperature in solvents commonly used for the elucidation of polymer microstructures and therefore it was not further studied.

In attempts to gain insight into the behavior of **4** in catalysis, its stoichiometric reactivity with various methylating agents (MeLi, MeMgCl) was pursued but led to intractable reaction mixtures. Additionally, after assuming that methylated species of type **6DFT** (Figure 6) could be a reasonable product from the reaction of **4** with MAO and a catalysis relevant precursor to the active species, its stability and plausible deactivation reactivity was investigated by computational means. In particular, the decomposition by migration of a methyl group from Ni to the C^{NHC} to **6DFTmig** was explored. This elementary step has been previously observed experimentally and/or implicated in the rigid pyridine dicarbene pincer ligands of the imidazol-2-ylidene type on a range of metals and with pincer ligands with bridgehead NHC donor.[18, 26]

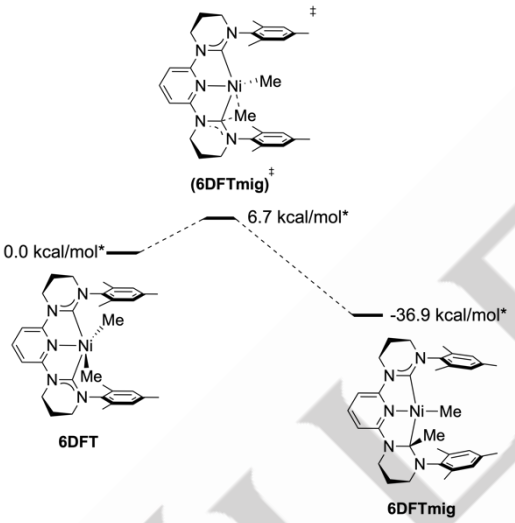

Figure 6. One plausible deactivation step of a catalysis relevant precursor **6DFT** *via* methyl migration into the Ni–C^{NHC} bond computed by DFT. *The numbers denote the Gibbs free energies (for the sake of comparison the reactant's energy was set to 0.0).

The results show that **6DFTmig** is very stable compared to **6DFT**; furthermore, it is accessible *via* a low energy barrier directly by concerted migration of one CH_3 from the Ni to the C^{NHC}.

Conclusion

The synthesis of the novel pyridine dicarbene pincer ligands, where the carbene is a RE-NHC, that are described herein, unraveled subtle electronic structure and steric profile differentiation from the established and widely studied analogues based on the imidazol-2-ylidenes. The donor-acceptor electronic characteristics of the new pincers stem from the nature of the constituent functional groups, while the steric profile is arising from conformational preferences of the ligand backbone on metal coordination. The diverse tuning handles in the ligand design promise to be useful for future applications in functional metal complexes. The computational studies have shown a gradual RE-NHC substituent and metal coligand dependent transition to pyramidalized four-coordinate Ni^{II} geometries, accompanied by triplet-singlet energy difference modulation. That the complexes **4** and **5a** show unremarkable catalytic activity in the oligo(poly)merization of ethylene may be attributed to catalyst deactivation due to migration elementary steps. The extension of the use of the novel pyridine RE-NHC pincer ligands to other metals and oxidation states, in particular 3d metals of relevance to catalysis, and the manipulation of singlet-triplet energy difference of pincer NHC complexes with potential applications in photocatalysis are directions that are currently under exploration.

Experimental Section

General experimental guidelines are given in the Supporting Information. Compound **2** was obtained by following a method of the literature (see Supporting Information).

Compound 3·HBr

To a round-bottom flask equipped with side-arm was added compound **2** (18.000 g, 50.828 mmol), $HC(OEt)_3$ (37.660 g, 254.140 mmol) and 2-3 drops conc. $HCOOH_{(aq)}$. With the side arm open, the mixture was stirred for 16 h at 100 °C, when a clear orange-red solution was obtained. After cooling to rt, diethyl ether was added and a sticky, off-white-to-orange solid precipitated, that was isolated by filtration and washed with diethyl ether affording a free-flowing solid. If the final solid product remains sticky (an indication of residual $HC(OEt)_3$ present), it is dried at 80-90 °C for *ca.* 16 h under vacuum. Yield: 7.197 g (50 %). ^{1}H-NMR (400 MHz, CD_3OD, 25 °C): δ = 8.17 (s, 1H, NC*H*N), 7.05 (s, 2H, *H*Ar), 3.69 (t, 2H, CH_2), 3.57 (t, 2H, CH_2), 2.31 (s, 3H, *p*-CH_3), 2.28 (m, 2H, CH_2), 2.26 (s, 6H, *o*-CH_3); ^{13}C{^{1}H}-NMR (100 MHz, CD_3OD, 25 °C): δ = 155.39 (N*C*HN), 141.32 (*C*Ar), 138.39 (*C*Ar), 136.11 (*C*Ar), 130.93 (*C*Ar), 47.70, 38.64, 21.00, 19.88, 17.49; HRMS (ESI): *m/z* calcd for $C_{13}H_{20}N_2Br$: 203.1543 $[M]^+$; found: 203.1556.

Compound 3

In two separate Schlenk flasks were added compound **3·HBr** (6.459 g, 22.806 mmol) in diethyl ether (*ca*. 50 mL) and ^{t}BuOK (2.815 g, 25.087 mmol) in diethyl ether (ca. 50 mL). After cooling the resulting mixtures to -10 °C, the base was added to the suspension of the salt and the mixture was stirred for 3-4 h at rt during which time the appearance of the precipitate changed. Removal of the precipitate by filtration through a pad of Celite and evaporation of the colourless filtrate under reduced pressure to dryness afforded the product as an off-white solid. Yield: 3.690 g (80 %). m.p. 100-103 °C; ^{1}H-NMR (400 MHz, $CDCl_3$, 25 °C): δ = 6.90 (s, 3H, *H*Ar & NC*HN*), 3.45 (t, 2H, CH_2), 3.33 (t, 2H, CH_2), 2.27 (s, 3H, p-CH_3), 2.22 (s, 6H, o-CH_3), 2.01 (m, 2H, CH_2);

$^{13}C\{^1H\}$-NMR (100 MHz, $CDCl_3$, 25 °C): δ = 149.41 (NC*H*N), 140.00 (*C*Ar), 137.46 (*C*Ar), 136.73 (*C*Ar), 129.42 (*C*Ar), 45.62, 43.28, 21.53, 21.02, 17.87; HRMS (ESI): *m/z* calcd for $C_{13}H_{19}N_2$: 203.1543 $[M+H]^+$; found: 203.1573.

(CHNCH)Br₂

In a small Schlenk flask were mixed as solids **3** (2.390 g, 11.814 mmol) and 2,6-dibromopyridine (1.399 g, 5.907 mmol). The mixture was placed under N_2, the vessel closed, *fully* immersed into an oil-bath and was left at 140 °C for 16 h during which time it gradually solidified to an off-white solid. After removal of the Schlenk from the oil bath, allowing it to cool to room temperature, breaking up the solid with a spatula and washing it with diethyl ether (3 x 20 mL), the product was obtained. Yield: 1.200 g (93%). ^1H-NMR (400 MHz, CD_3CN, 25 °C): δ = 9.11 (s, 2H, NC*H*N), 8.18 (t, $^3J_{H,H}$=8.13 Hz, 1H, p-C*H*pyr), 7.46-7.44 (d, $^3J_{H,H}$=8.22 Hz, 2H, m-C*H*pyr), 7.04 (s, 4H, *H*Ar), 4.12 (t, 4H, CH_2), 3.77 (t, 4H, CH_2), 2.43 (m, 4H, CH_2), 2.31 (s, 6H, p-CH_3), 2.22 (s, 12H, o-CH_3); $^{13}C\{^1H\}$-NMR (100 MHz, CD_3CN, 25 °C): δ = 153.85 (NC*H*N), 150.82 (*C*Ar), 144.45 (*C*Ar), 141.36 (*C*Ar), 137.96 (*C*Ar), 135.47 (*C*Ar), 130.70 (*C*Ar), 112.43 (*C*Ar), 48.25, 43.97, 20.97, 19.63, 17.80; MS (50 eV): *m/z* (%): 240 (26) $[M]^{2+}$, 560 (16) $[M+^{79}Br]^+$, 562 (16) $[M+^{81}Br]^+$, 498 (100) $[M+H_2O]^+$; HRMS (ESI): *m/z* calcd for $C_{31}H_{39}N_5Br_2$: 240.6597 $[M]^{2+}$; found: 240.6598.

(CH^N^CH)Br₂

In a round-bottom flask were added 0.392 g (1.483 mmol) of 2,6-bis(bromomethyl)pyridine and 0.600 g (2.966 mmol) of **3**. After addition of dry CH_3CN (20 mL) the mixture was stirred at rt for 16 h during which time a suspension had formed. Volatiles were removed under reduced pressure, the white solid residue was washed with diethyl ether and dried under vacuum. Yield: 0.694 g, (70%). ^1H-NMR (400 MHz, $CDCl_3$, 25 °C): δ = 9.24 (s, 2H, NCHN), 7.72-7.69 (t, $^3J_{H,H}$=7.69 Hz, 1H, p-CHpyr), 7.56-7.55 (d, $^3J_{H,H}$=7.64 Hz, 2H, m-CHpyr), 6.89 (s, 4H, HAr), 5.33 (s, 4H, CH_2), 3.66 (t, 4H, CH_2), 3.61 (t, 4H, CH_2), 2.32-2.29 (br, 4H, CH_2), 2.26 (m, 18H, o-CH_3 & p-CH_3); $^{13}C\{^1H\}$-NMR (100 MHz, $CDCl_3$, 25 °C): δ = 155.19 (NCHN), 154.08 (CAr), 139.99 (CAr), 138.89 (CAr), 136.44 (CAr), 134.50 (CAr), 130.19 (CAr), 123.27 (CAr), 59.38, 46.24, 44.48, 21.12, 19.49, 18.25; MS (25 eV): *m/z* (%): 508 (14) $[M]^+$, 254 (74) $[M]^{2+}$, 588 (100) $[M+^{79}Br]^+$, 590 (100) $[M+^{81}Br]^+$; HRMS (ESI): *m/z* calcd for $C_{33}H_{43}N_5Br_2$: 254.6754 $[M]^{2+}$; found: 254.6758.

***In Situ* Generation and Characterization of the CNC**

In a Young NMR-tube were placed **(CHNCH)Br₂** (0.025 g, 0.039 mmol) and NaHMDS (0.016 g, 0.085 mmol). The tube was cooled at -30 °C, C_6D_6 (0.6 mL) was added and the mixture was left to reach rt while manually agitating for 30 min. Finally, the ^1H- and $^{13}C\{^1H\}$-NMR spectra of the reaction mixture were recorded; the spectra demonstrated the formation of a single product corresponding to the **CNC**, despite the fact that an anticipated downfield signal in the $^{13}C\{^1H\}$-NMR spectrum assignable to C^{NHC} could not be observed. The spectrum remained unchanged for at least 24 h. ^1H-NMR (400 MHz, C_6D_6, 25 °C): δ = 7.08 (br, 3H, *p*-C*H*pyr and *m*-C*H*pyr), 6.70 (s, 4H, *H*Ar), 3.37 (br, 4H, CH_2), 2.69 (br, 4H, CH_2), 2.14-2.12 (m, 18H, *o*-CH_3 and *p*-CH_3), 1.65 (br, 4H, CH_2); $^{13}C\{^1H\}$-NMR (100 MHz, C_6D_6, 25 °C): δ = 157.84 (CAr), 144.54 (CAr), 139 (CAr), 136.67 (CAr), 134.10 (CAr), 129.70 (CAr), 105.84 (CAr), 44.27, 39.30, 21.58, 21.07, 18.01, 6.56.

Complex 4

In a Schlenk flask were added NaHMDS (0.075 g, 0.411 mmol) and **(CHNCH)Br₂** (0.120 g, 0.187 mmol). After cooling the mixture of the solids to -78 °C, THF *(ca.* 20 mL) was added and the suspension was stirred for 2 h reaching rt, when it assumed a yellow coloration; subsequently, it was added dropwise to a dark green solution of $[NiBr_2(PPh_3)_2]$ (0.139 g, 0.187 mmol) in THF (10 mL), affording an orange suspension that was stirred for 16 h at rt. Evaporation of the volatiles under reduced pressure, washing of the solid residue with toluene (3 x 15 mL), extraction into CH_2Cl_2 (*ca.* 20 mL) and filtration through a pad of Celite afforded a clear orange filtrate from which **4** was obtained as an orange solid after removing the volatiles under reduced pressure. Yield: 0.078 g (60%). Orange crystals of **4** suitable for SC-XRD were obtained by slow diffusion of toluene to a CH_2Cl_2 solution at room temperature. ^1H-NMR (400 MHz, $CDCl_3$, 25 °C): δ = 8.08 (t, 1H, *p*-C*H*pyr), 7.03-7.01 (d, 2H, *m*-C*H*pyr), 6.72 (s, 4H, *H*Ar), 3.92 (t, 4H, CH_2), 3.47 (t, 4H, CH_2), 2.39 (s, 12H, o-CH_3), 2.37 (m, 4H, CH_2), 2.23 (s, 6H, *p*-CH_3).

Complexes 5a and 5b

Inside a N_2 filled glove box in a Schlenk flask were placed **(CHNCH)Br₂** (0.185 g, 0.289 mmol) and THF (10 mL) giving an off-white suspension. To this was added $[Cr\{N(SiMe_3)_2\}_2(THF)_2]$ (0.178 g, 0.346 mmol) and the mixture was stirred for 16 h at rt, during which time a grey suspension and $HN(SiMe_3)_2$ were formed. The volatiles were removed under reduced pressure, the solid residue was removed from the glove box and washed with ether. Although the nature of the metal species at this stage was unknown, the residue was extracted into CH_2Cl_2 giving a light-brown solution. It is plausible that CH_2Cl_2 may act as one electron oxidant which could account for the formation of **5a**. Evaporation of all volatiles under reduced pressure afforded a light-brown solid which upon washing with THF turned pink purple. The evaporation step after the extraction with CH_2Cl_2 must be performed rapidly in order to suppress formation of **5b** by halogen exchange with the solvent. After drying the residue under vacuum, analytically pure **5a** was obtained. Yield: 0.127 g (57%). Pink purple crystals of **5b** suitable for SC-XRD were grown by slow diffusion of pentane to a CH_2Cl_2 solution at room temperature over one week. Elemental analysis, calcd (%) for $C_{31}H_{37}Br_3CrN_5$: C 48.27, H 4.83, N 9.08; found: C 48.14, H 5.60, N 8.77.

General Procedure for Ethylene Oligomerization and Polymerization Catalysis

The catalytic reactions were performed in a magnetically stirred (1200 rpm) 145 mL stainless steel autoclave. A 125 mL glass container was used to avoid corrosion of the autoclave walls. The precatalyst solution was prepared by dissolving 1 x 10^{-5} mol of the complex in chlorobenzene. This solution was injected into the reactor under an ethylene flux, followed by the cocatalyst solution

(400 equiv. of MAO in toluene). After injection of the catalyst and cocatalyst solutions under a constant low flow of ethylene, which is considered as the t_0 time, the reactor was immediately pressurized to 10 bar of ethylene. The 10 bar working pressure was maintained through a continuous feed of ethylene from a bottle placed on a balance to allow monitoring of the ethylene uptake. The reaction mixture was stirred for the given reaction time. At the end of each test, a dry ice bath was used to rapidly cool the reactor. When the inner temperature reached 0 °C, the ice bath was removed, allowing the temperature to slowing rise to 18 °C. The gaseous phase was then transferred into a 10 L polyethylene tank filled with water. An aliquot of this gaseous phase was transferred into a Schlenk flask, previously evacuated, for GC analysis. The amount of ethylene consumed was thus determined by differential weighting of the bottle (accuracy of the scale: 0.001 g). To this amount of ethylene, the remaining ethylene (calculated using the GC analysis) in the gaseous phase was subtracted. The reaction mixture in the reactor was quenched *in situ* by the addition of ethanol (10 mL), transferred into a Schlenk flask, and separated from the metal complexes by trap-to-trap evaporation into a second Schlenk flask previously immersed in liquid N_2 to avoid loss of product for GC analysis. The liquid phase was analyzed by GC, whereas the solid phase (when polymers are formed) was washed several times with a 1:1 mixture of ethanol/HCl before being weighted. Analysis of the solid polyethylene phase by GPC or NMR was not possible due to the poor solubility of the former in commonly utilized solvents. Each catalytic test was performed at least twice to ensure the reproducibility of the results.

Supporting Information

General experimental guidelines, methodology and spectroscopic data, crystallographic data and computational details are given in the Supporting Information. The authors have cited additional references within the Supporting Information.

Acknowledgements

The Special Accounts for Research Grants (S.A.R.G.) of the National and Kapodistrian University of Athens (NKUA) for the provision of partial support, access to the single crystal X-ray Diffractometer of the Core Facility at NKUA and the HPC of the University of Strasbourg for computational time are gratefully acknowledged. We thank the CNRS and the MESRI (Paris) for support (P.B., D.A., K. P.). We also thank Dr. E. Sakki for carrying out mass spectroscopic measurements and Fani Kournavou for the design of the Table of Contents/Abstract graphic.

Keywords: Pincer• Nickel • Chromium• Oligomerization• N-heterocyclic Carbene.

Entry for the Table of Contents

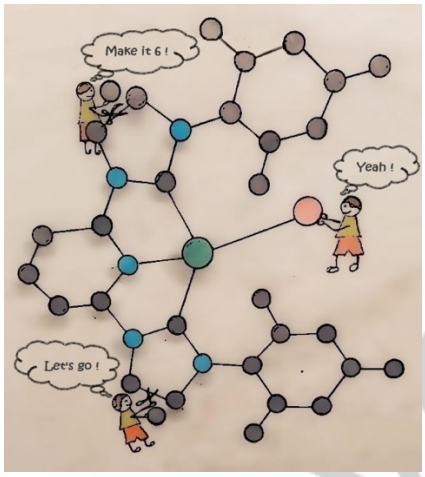

Pyridine Ring-Expanded dicarbene Pincer ligands were synthesized and some representative complexes with Ni and Cr show distinct geometrical and electronic characteristics from analogues with 5-membered ring heterocycles, opening new possibilities for pincer ligands featuring carbene donors.

[1] a) D. Pugh, A. A. Danopoulos, *Coord. Chem. Rev.* **2007**, *251*, 610-641; b) D. Zhang, G. Zi, *Chem. Soc. Rev.* **2015**, *44*, 1898-1921; c) R. E. Andrew, L. González-Sebastián, A. B. Chaplin, *Dalton Trans.* **2016**, *45*, 1299-1305; d) Y. Liu, P. Persson, V. Sundström, K. Wärnmark, *Acc. Chem. Res.* **2016**, *49*, 1477-1485; e) S. Hameury, P. de Frémont, P. Braunstein, *Chem. Soc. Rev*. **2017**, 46, 632-733; f) V. Charra, P. de Frémont, P. Braunstein, *Coord. Chem. Rev*. **2017**, *341*, 53-176; g) A. A. Danopoulos, T. Simler, P. Braunstein, *Chem. Rev.* **2019**, *119*, 3730-3961; h) R. Arevalo, P. J. Chirik, *J. Am. Chem. Soc.* **2019**, *141*, 9106-9123; i) Q. Liang, D. Song, *Chem. Soc. Rev.* **2020**, *49*, 1209-1232; j) V. Arora, H. Narjinari, P. G. Nandi, A. Kumar, *Dalton Trans.* **2021**, *50*, 3394-3428; k) Y. Wang, B. Zhang, S. Guo, *Eur. J. Inorg. Chem.* **2021**, *2021*, 188-204; l) A. A. Danopoulos, T. Simler, P. Braunstein, in "*Comprehensive Organometallic Chemistry IV*" (*COMC-IV*), K. Meyer, D. O'Hare, G. Parkin (Editors-in-Chief); T. H. Warren (Section Editor), Elsevier, **2022**, Vol. 7.11, pp 632–758; m) I. Ligielli, A. A. Danopoulos, P. Braunstein, T. Simler, in "*Comprehensive Organometallic Chemistry IV*" (*COMC-IV*), K. Meyer, D. O'Hare, G. Parkin (Editors-in-Chief); T. H. Warren (Section Editor), Elsevier, **2022**, Vol. 8.07, pp 427–574; n) F. He, K. P. Zois, D. Tzeli, A. A. Danopoulos, P. Braunstein, *Coord. Chem. Rev.* **2024**, *XXXX*, XXXX.

[2] a) A. Melaiye, R. S. Simons, A. Milsted, F. Pingitore, C. Wesdemiotis, C. A. Tessier, W. J. Youngs, *J. Med. Chem.* **2004**, *47*, 973-977; b) D. van der Westhuizen, C. A. Slabber, M. A. Fernandes, D. F. Joubert, G. Kleinhans, C. J. van der Westhuizen, A. Stander, O. Q. Munro, D. I. Bezuidenhout, *Chem. Eur. J.* **2021**, *27*, 8295-8307.

[3] a) H. V. Huynh, *Chem. Rev.* **2018**, *118*, 9457-9492; b) D. Munz, *Organometallics* **2018**, *37*, 275-289; c) L. Falivene, Z. Cao, A. Petta, L. Serra, A. Poater, R. Oliva, V. Scarano, L. Cavallo, *Nat. Chem.* **2019**, *11*, 872-879.

[4] D. M. Andrada, N. Holzmann, T. Hamadi, G. Frenking, *Beilstein J. Org. Chem.* **2015**, *11*, 2727-2736.

[5] a) M. Melaimi, R. Jazzar, M. Soleilhavoup, G. Bertrand, *Angew. Chem. Int. Ed.* **2017**, *56*, 10046-10068; b) A. Vivancos, C. Segarra, M. Albrecht, *Chem. Rev.* **2018**, *118*, 9493-9586.

[6] a) A. Eizawa, K. Arashiba, H. Tanaka, S. Kuriyama, Y. Matsuo, K. Nakajima, K. Yoshizawa, Y. Nishibayashi, *Nat. Commun.* **2017**, *8*, 14874; b) A. Egi, H. Tanaka, A. Konomi, Y. Nishibayashi, K. Yoshizawa, *Eur. J. Inorg. Chem.* **2020**, *2020*, 1490-1498; c) S. Takaoka, A. Eizawa, S. Kusumoto, K. Nakajima, Y. Nishibayashi, K. Nozaki, *Organometallics* **2018**, *37*, 3001-3009.

[7] R. Maity, B. Sarkar, *JACS Au* **2022**, *2*, 22-57.

[8] T.-a. Koizumi, T. Tomon, K. Tanaka, *Organometallics* **2003**, *22*, 970-975.

[9] J. Long, D. M. Lyubov, G. A. Gurina, Y. V. Nelyubina, F. Salles, Y. Guari, J. Larionova, A. A. Trifonov, *Inorg. Chem.* **2022**, *61*, 1264-1269.

[10] a) V. Friese, S. Nag, J. Wang, M.-P. Santoni, A. Rodrigue-Witchel, G. S. Hanan, F. Schaper, *Eur. J. Inorg. Chem.* **2011**, *2011*, 39-44; b) J. A. Thagfi, G. G. Lavoie, *Organometallics* **2012**, *31*, 7351-7358; c) H. Z. Kaplan, B. Li, J. A. Byers, *Organometallics* **2012**, *31*, 7343-7350; d) R. M. Brown, J. Borau Garcia, J. Valjus, C. J. Roberts, H. M. Tuononen, M. Parvez, R. Roesler, *Angew. Chem. Int. Ed.* **2015**, *54*, 6274-6277; e) Y. Jiang, C. Gendy, R. Roesler, *Organometallics* **2018**, *37*, 1123-1132.

[11] F. He, C. Gourlaouen, H. Pang, P. Braunstein, *Chem. Eur. J.* **2022**, *28*, e202104234.

[12] R. P. Yu, J. M. Darmon, C. Milsmann, G. W. Margulieux, S. C. E. Stieber, S. DeBeer, P. J. Chirik, *J. Am. Chem. Soc.* **2013**, *135*, 13168-13184.

[13] a) T. Simler, P. Braunstein, A. A. Danopoulos, *Organometallics* **2016**, *35*, 4044-4049; b) X. Ren, C. Gourlaouen, M. Wesolek, P. Braunstein, *Angew. Chem. Int. Ed.* **2017**, *56*, 12557-12560; c) Y. Li, K. Pelzer, D. Sechet, G. Creste, D. Matt, P. Braunstein, D. Armspach, *Dalton Trans.* **2022**, *51*, 11226-11230; d) F. He, C. Gourlaouen, H. Pang, P. Braunstein, **2022**, *28*, e202104234.

[14] Deposition Numbers <url href="https://www.ccdc.cam.ac.uk/services/structures?id=doi:10.1002/asia.202400169R1"> 2328279 (for **4**), 2328280 (for **5b**) </url> contain the supplementary crystallographic data for this paper. These data are provided free of charge by the joint Cambridge Crystallographic Data Centre and Fachinformationszentrum Karlsruhe <url href="http://www.ccdc.cam.ac.uk/structures"> Access Structures service</url>.

[15] G. Leniec, *ACS Appl. Opt. Mater.* **2023**, *1*, 1114-1121.

[16] L. Yang, D. R. Powell, R. P. Houser, *Dalton Trans.* **2007**, 955-964.

[17] K. Inamoto, J.-i. Kuroda, K. Hiroya, Y. Noda, M. Watanabe, T. Sakamoto, *Organometallics* **2006**, *25*, 3095-3098.

[18] D. Pugh, A. Boyle, A. A. Danopoulos, *Dalton Trans.* **2008**, 1087-1094.

[19] K. Inamoto, J.-i. Kuroda, E. Kwon, K. Hiroya, T. Doi, *J. Organomet. Chem.* **2009**, *694*, 389-396.

[20] D. H. Brown, B. W. Skelton, *Dalton Trans.* **2011**, *40*, 8849-8858.

[21] D. S. McGuinness, V. C. Gibson, D. F. Wass, J. W. Steed, *J. Am. Chem. Soc.* **2003**, *125*, 12716-12717.

[22] D. Pugh, J. A. Wright, S. Freeman, A. A. Danopoulos, *Dalton Trans.* **2006**, 775-782.

[23] a) T. Agapie, *Coord. Chem. Rev.* **2011**, *255*, 861-880; b) H. Olivier-Bourbigou, P. A. R. Breuil, L. Magna, T. Michel, M. F. Espada Pastor, D. Delcroix, *Chem. Rev.* **2020**, *120*, 7919-7983; c) N. Patel, V. Valodkar, G. Tembe, *Polymer Chemistry* **2023**, *14*, 2542-2571.

[24] D. S. McGuinness, V. C. Gibson, J. W. Steed, *Organometallics* **2004**, *23*, 6288-6292.

[25] V. C. Gibson, S. K. Spitzmesser, *Chem. Rev.* **2003**, *103*, 283-316.

[26] a) A. A. Danopoulos, N. Tsoureas, J. C. Green, M. B. Hursthouse, *Chem. Commun.* **2003**, 756-757; b) C. Romain, D. Specklin, K. Miqueu, J.-M. Sotiropoulos, C. Fliedel, S. Bellemin-Laponnaz, S. Dagorne, *Organometallics* **2015**, *34*, 4854-4863; c) E. Despagnet-Ayoub, M. K. Takase, J. A. Labinger, J. E. Bercaw, *J. Am. Chem. Soc.* **2015**, *137*, 10500-10503.